RESEARCH ARTICLE SUMMARY

GEOMORPHOLOGY

Geomorphic and geologic controls of geohazards induced by Nepal's 2015 Gorkha earthquake

J. S. Kargel,*† G. J. Leonard,* D. H. Shugar,*† U. K. Haritashya,*† A. Bevington, E. J. Fielding, K. Fujita, M. Geertsema, E. S. Miles, J. Steiner, E. Anderson, S. Bajracharya, G. W. Bawden, D. F. Breashears, A. Byers, B. Collins, M. R. Dhital, A. Donnellan, T. L. Evans, M. L. Geai, M. T. Glasscoe, D. Green, D. R. Gurung, R. Heijenk, A. Hilborn, K. Hudnut, C. Huyck, W. W. Immerzeel, Jiang Liming, R. Jibson, A. Kääb, N. R. Khanal, D. Kirschbaum, P. D. A. Kraaijenbrink, D. Lamsal, Liu Shiyin, Lv Mingyang, D. McKinney, N. K. Nahirnick, Nan Zhuotong, S. Ojha, J. Olsenholler, T.H. Painter, M. Pleasants, K. C. Pratima, Q. I. Yuan, B. H. Raup, D. Regmi, D. R. Rounce, A. Sakai, Shangguan Donghui, J. M. Shea, A. B. Shrestha, A. Shukla, D. Stumm, M. van der Kooij, K. Voss, Wang Xin, B. Weihs, D. Wolfe, Wu Lizong, Yao Xiaojun, M. R. Yoder, N. Young

INTRODUCTION: On 25 April 2015, the Gorkha earthquake [magnitude (*M*) 7.8] struck Nepal, followed by five aftershocks of ≥*M* 6.0 until 10 June 2015. The earthquakes killed ~9000 people and severely damaged a 550 by 200 km region in Nepal and neighboring countries. Some mountain villages were completely destroyed, and the remote locations, blocked roads, and landslide-dammed rivers prevented ground access to many areas.

RATIONALE: Our "Volunteer Group" of scientists from nine nations, motivated by humanitarian needs, focused on satellite-based systematic mapping and analysis of earthquake-induced geohazards. We provided information to relief and recovery officials as emergency operations were occurring, while supported by one of the largest-ever NASA-led campaigns of responsive satellite data acquisitions over a vast disaster zone. Our analysis of geohazards distribution allowed evaluation of geomorphic, tectonic, and lithologic controls on earthquake-induced landsliding, process mechanisms, and hazard process chains, particularly where they affected local populations.

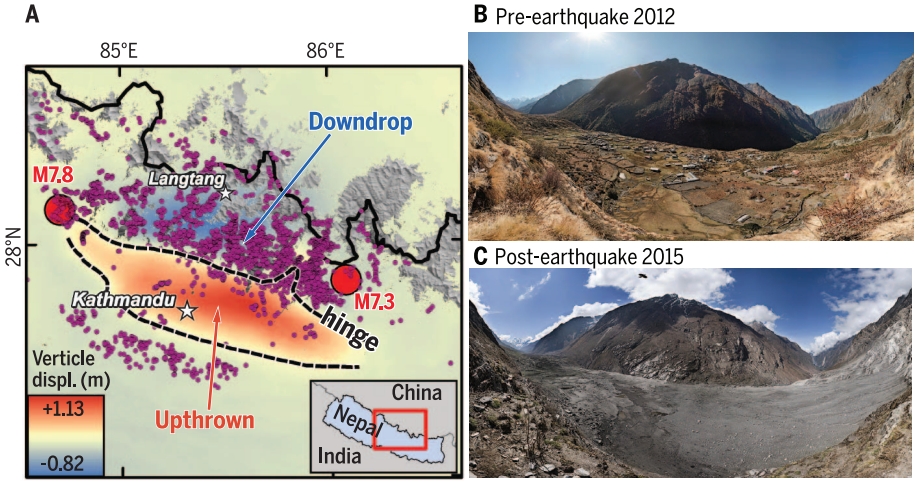

Landslide distribution and effects of a huge landslide. (**A**) Landslides (purple dots) are concentrated mostly north of the tectonic hinge-line. Also shown are the epicenters of the main shock and largest aftershock. Displacements are from the JAXA ALOS-2 ScanSAR interferogram (21 Feb and 2 May 2015 acquisitions). (**B** and **C**) Before-and-after photographs obtained by D. Breashears in Langtang Valley showing complete destruction of a large part of Langtang village by a huge landslide.

RESULTS: We mapped 4312 coseismic and postseismic landslides. Their distribution shows positive associations with slope and shaking intensity. The highest areal densities of landslides are developed on the downdropped northern tectonic block, which is likely explained by momentary reduction of the normal stress along planes of weakness during downward acceleration. The two largest shocks bracket the high-density landslide distribution, the largest magnitudes of the surface displacement field, and highest peak ground accelerations (PGAs). Landslides are heavily concentrated where PGA was >0.6*g* and slope is >30°. Additional controls on landslide occurrence are indicated by their clustering near earthquake epicenters and within specific lithologic units. The product of PGA and the sine of surface slope (defined as the landslide susceptibility index) is a good indicator of where most landslides occurred. A tail of the statistical distributions of landslides extends to low values of the landslide susceptibility index. Slight earthquake shaking affected vulnerable materials hanging on steep slopes—such as ice, snow, and glacial debris—and moderate to strong shaking affected poorly consolidated sediments deposited in low-sloping river valleys, which were already poised near a failure threshold. In the remote Langtang Valley, some of the most concentrated destruction and losses of life outside the Kathmandu Valley were directly due to earthquake-induced landslides and air blasts. Complex seismic wave interactions and wave focusing may have caused ridgetop shattering and landslides near Langtang but reduced direct shaking damage on valley floors and at glacial lakes.

ON OUR WEB SITE

Read the full article at http://dx.doi.org/10.1126/science.aac8353

CONCLUSION: The Gorkha earthquake took a tremendous, tragic toll on human lives and culture. However, fortunately no damaging earthquake-caused glacier lake outburst floods were observed by our satellite analysis. The total number of landslides was far fewer than those generated by comparable earthquakes elsewhere, probably because of a lack of surface ruptures, the concentration of deformation along the subsurface thrust fault at 10 to 15 km depth, and the regional dominance of competent high-grade metamorphic and intrusive igneous rock types. ■

The list of author affiliations is available in the full article online.
*These authors contributed equally to this work.
†Corresponding author. E-mail: kargel@hwr.arizona.edu (J.S.K.); dshugar@uw.edu (D.H.S.); uharitashya1@udayton.edu (U.K.H.)
Cite this article as J. S. Kargel *et al.*, *Science* **351**, aac8353 (2016). DOI: 10.1126/science.aac8353

RESEARCH ARTICLE

GEOMORPHOLOGY

Geomorphic and geologic controls of geohazards induced by Nepal's 2015 Gorkha earthquake

J. S. Kargel,[1]*† G. J. Leonard,[1]* D. H. Shugar,[2]*† U. K. Haritashya,[3]*† A. Bevington,[4] E. J. Fielding,[5] K. Fujita,[6] M. Geertsema,[4] E. S. Miles,[7] J. Steiner,[8] E. Anderson,[9] S. Bajracharya,[10] G. W. Bawden,[11] D. F. Breashears,[12] A. Byers,[13] B. Collins,[14] M. R. Dhital,[15] A. Donnellan,[5] T. L. Evans,[16] M. L. Geai,[17] M. T. Glasscoe,[5] D. Green,[11] D. R. Gurung,[10] R. Heijenk,[4] A. Hilborn,[16] K. Hudnut,[18] C. Huyck,[19] W. W. Immerzeel,[20] Jiang Liming,[21] R. Jibson,[22] A. Kääb,[23] N. R. Khanal,[10] D. Kirschbaum,[24] P. D. A. Kraaijenbrink,[20] D. Lamsal,[5] Liu Shiyin,[25] Lv Mingyang,[26] D. McKinney,[27] N. K. Nahirnick,[16] Nan Zhuotong,[28] S. Ojha,[5] J. Olsenholler,[29] T. H. Painter,[5] M. Pleasants,[3] K. C. Pratima,[30] Q. I. Yuan,[25] B. H. Raup,[31] D. Regmi,[32] D. R. Rounce,[33] A. Sakai,[6] Shangguan Donghui,[25] J. M. Shea,[10] A. B. Shrestha,[10] A. Shukla,[34] D. Stumm,[10] M. van der Kooij,[35] K. Voss,[36] Wang Xin,[37] B. Weihs,[38] D. Wolfe,[39] Wu Lizong,[26] Yao Xiaojun,[40] M. R. Yoder,[41] N. Young[42]

The Gorkha earthquake (magnitude 7.8) on 25 April 2015 and later aftershocks struck South Asia, killing ~9000 people and damaging a large region. Supported by a large campaign of responsive satellite data acquisitions over the earthquake disaster zone, our team undertook a satellite image survey of the earthquakes' induced geohazards in Nepal and China and an assessment of the geomorphic, tectonic, and lithologic controls on quake-induced landslides. Timely analysis and communication aided response and recovery and informed decision-makers. We mapped 4312 coseismic and postseismic landslides. We also surveyed 491 glacier lakes for earthquake damage but found only nine landslide-impacted lakes and no visible satellite evidence of outbursts. Landslide densities correlate with slope, peak ground acceleration, surface downdrop, and specific metamorphic lithologies and large plutonic intrusions.

On 25 April 2015 and over the next several weeks, a major series of displacements occurred ~15 km deep along the buried Main Himalayan Thrust without breaking the surface (*1*–*3*). The main shock of the Gorkha earthquake [magnitude (*M*) 7.8, U.S. Geological Survey (USGS); epicenter 28.147°N, 84.708°E] was followed by ~257 aftershocks of >*M* 3.0, including five ≥*M* 6.0 between 25 April and 10 June 2015. On 12 May, a *M* 7.3 aftershock struck ~150 km ENE of the main shock. The largest earthquakes caused a wide swath of casualties and destruction in Nepal and adjacent India, China, and Bangladesh. Some mountain villages were shaken to complete destruction (*4*), buried by avalanches and landslides, or destroyed by powerful avalanche and landslide air blasts. The remote locations and blocked roads and rivers meant that ground crews could not immediately access many Himalayan valleys.

We adopted a satellite-based approach to examine the vast damaged region. Satellite imagery was provided by NASA, DigitalGlobe, the Japan Aerospace Exploration Agency (JAXA), MacDonald Dettwiler and Associates (MDA), Planet Labs, Spot Image, and the China National Space Administration, including imagery triggered by the International Charter: Space and Major Disasters (www.disasterscharter.org). A "Volunteer Group" of analysts from nine nations was organized by the University of Arizona under the auspices of Global Land Ice Measurements from Space (GLIMS) (*5*) initially to assess priority hazard situations and then to build a landslide inventory (*6*). The group contributed their input of mapped geohazards to a broad ad hoc NASA-led interagency "Response Team." We scrutinized optical imagery, ranging from 15 to <1 m resolution, from Landsats 7 and 8; the Advanced Spaceborne and Thermal Emission and Reflection Radiometer (ASTER) onboard Terra; Advanced Land Imager on EO-1; WorldView-1, -2, and -3; GeoEye-1; Pleiades; and Gaofen-1 (table S1) and used radar data from ALOS-2 and RADARSAT-2 and topography from the Shuttle Radar Topography Mission (SRTM). Landslides not detectable at these scales would generally have lesser human consequences than would larger landslides.

The Response Team, including the Volunteer Group, undertook one of the broadest and fastest international emergency remote sensing and data analysis campaigns ever led by NASA for any earthquake-affected region (*7*–*9*). Parallel, but independent, landslide-mapping efforts have been undertaken by a joint British Geological Survey–Durham University group (*10*) and other groups.

During previous earthquake emergencies in mountainous terrain (such as Wenchuan, China and Denali, Alaska), landslides were numerous (*9*, *11*–*17*), sometimes initiating a process chain of secondary and tertiary geomorphic processes over time spans ranging from minutes to years after the earthquake (*18*, *19*). Landslide-initiated process chains may involve gains in mobilized mass and destructive power through energy and mass transfer cascades. Many documented or inferred examples exist, including rock/ice fall–generated debris avalanches that transformed into debris flows (*20*, *21*) or caused large impoundment lakes and upstream flooding (*22*), landslide-generated displacement waves and glacier lake

[1]Department of Hydrology and Water Resources, University of Arizona, Tucson, AZ, USA. [2]School of Interdisciplinary Arts and Sciences, University of Washington Tacoma, Tacoma, WA, USA. [3]Department of Geology, University of Dayton, Dayton, OH, USA. [4]Ministry of Forests, Lands and Natural Resource Operations, Prince George, BC, Canada. [5]Jet Propulsion Laboratory, California Institute of Technology, Pasadena, CA, USA. [6]Graduate School of Environmental Studies, Nagoya University, Nagoya, Japan. [7]Scott Polar Research Institute, University of Cambridge, Cambridge, UK. [8]Institute of Environmental Engineering, Federal Institute of Technology–ETH, Zurich, Switzerland. [9]NASA Marshall Space Flight Center, Huntsville, AL, USA. [10]International Centre for Integrated Mountain Development, Kathmandu, Nepal. [11]NASA Headquarters, Washington, DC, USA. [12]GlacierWorks, Marblehead, MA, USA. [13]The Mountain Institute, Elkins, WV, USA. [14]U.S. Geological Survey, Menlo Park, CA, USA. [15]Central Department of Geology, Tribhuvan University, Kirtipur, Kathmandu, Nepal. [16]Department of Geography, University of Victoria, Victoria, BC, Canada. [17]CVA Engineering, Suresnes, France. [18]Earthquake Science Center, U.S. Geological Survey, Pasadena, CA, USA. [19]ImageCat, Long Beach, CA, USA. [20]Faculty of Geosciences, Utrecht University, Utrecht, Netherlands. [21]State Key Laboratory of Geodesy and Earth's Dynamics, Institute of Geodesy and Geophysics, Chinese Academy of Sciences, Wuhan, Hubei Province, China. [22]U.S. Geological Survey, Golden, CO, USA. [23]Department of Geosciences, University of Oslo, Blindern, Oslo, Norway. [24]Hydrological Sciences Laboratory, NASA Goddard Space Flight Center, Greenbelt, MD, USA. [25]Cold and Arid Regions of Environmental and Engineering Research Institute, Chinese Academy of Sciences, Lanzhou, China. [26]School of Earth Sciences and Engineering, Nanjing University, Nanjing, China. [27]Department of Civil, Architectural and Environmental Engineering, University of Texas at Austin, Austin, TX, USA. [28]School of Geography Science, Nanjing Normal University, Nanjing, China. [29]Department of Geography, Texas A&M University, College Station, TX, USA. [30]Arizona Remote Sensing Center, School of Natural Resources and the Environment, University of Arizona, Tucson, AZ, USA. [31]National Snow and Ice Data Center, University of Colorado, Boulder, CO, USA. [32]Himalayan Research Center, Kathmandu, Nepal. [33]Environmental and Water Resources Engineering, University of Texas at Austin, Austin, TX, USA. [34]Wadia Institute of Himalayan Geology, Dehradun, India. [35]MacDonald Dettwiler and Associates–GSI, Ottawa, Ontario, Canada. [36]Department of Geography, University of California, Santa Barbara, Santa Barbara, CA, USA. [37]College of Architecture and Urban Planning, Hunan University of Science and Technology, Xiangtan, China. [38]Geography Department, Kansas State University, Manhattan, KS, USA. [39]**Global Land Ice Measurements from Space** (GLIMS) Steward, Alaska Region, Anchorage, AK, USA. [40]College of Geographical Science and Environment, Northwest Normal University, China. [41]Department of Physics, University of California, Davis, Davis, CA, USA. [42]Antarctic Climate and Ecosystems Cooperative Research Centre, University of Tasmania, Hobart, TAS, Australia.

*These authors contributed equally to this work. **†Corresponding author. E-mail: kargel@hwr.arizona.edu (J.S.K.); dshugar@uw.edu (D.H.S.); uharitashya1@udayton.edu (U.K.H.)**

outburst floods (GLOFs) (23, 24), and landslide-dammed lake outbursts (25, 26). As debris, ice, and lake and stream water are ingested into an outburst flood, a debris flow or hyper-concentrated slurry flood may result (21). Each geomorphic process in the chain may trigger a subsequent geohazard and extend the damaging reach of the event (27, 28). Process chains involving GLOFs are particularly worrisome.

The Volunteer Group's work focused on systematic mapping of quake-induced geohazards, understanding the geomorphic, lithologic, and tectonic control of their distribution and the identification of communities and infrastructure that might be affected. We analyzed the distribution and character of the geohazards induced by the Gorkha earthquake in Nepal and Tibet using mainly satellite-based findings, supplemented with media reports, eyewitness photography, helicopter-borne field assessments, and modeling of lake outburst flood processes. This paper considers earthquake-related landslides formed before 10 June 2015, when the monsoon arrived in eastern Nepal.

Landslide mapping and assessment

We mapped the distribution of 4312 earthquake-induced (coseismic and postseismic) landslides (Fig. 1). We identified six Areas of Interest (AOIs) that include Annapurna, Manaslu, Ganesh Himal, Langtang, Cho Oyu, and Everest (fig. S1) from west to east. The AOIs together cover 375 by 155 km, with divisions set along major valleys. Each AOI team had remote sensing and landslide expertise and was assigned an experienced lead analyst.

Multispectral satellite images from many government and commercial sensors (table S1) were made available through a number of portals, including the DigitalGlobe website, the USGS Hazards Data Distribution System (HDDS), and USGS Global Visualization Viewer (GLOVIS). Additionally, NASA provided access to expedited post-earthquake targeted ASTER imagery within the affected region. Not all locations were surveyed repetitively. We compiled a database and detailed descriptions of each AOI (29).

The highest densities of earthquake-related landslides are distributed in a broad swath between the two largest shocks, where many aftershocks also occurred. Clusters of landslides also exist outside of this zone (Fig. 1). The high landslide densities also lie between three >M 7.0 earthquakes that occurred on 26 August 1833, 25 April 2015, and 12 May 2015, thus highlighting the possible long-term effects of historic quakes. However, we assessed the landslide occurrences only within the context of the Gorkha earthquake and aftershocks and the terrain characteristics, broadly organized according to (i) surface slopes and the earthquakes' seismic peak ground accelerations (PGAs), (ii) broad-field deformation due to the earthquakes, and (iii) the distribution of underlying landcover, lithology, and tectonic structure.

Among the shaking parameters, PGA is just one factor that may control whether landslides occur in response to an earthquake. The specific frequency content, shake duration, PGA direction, and recurrent shocks also may be important (30). Furthermore, the landslides caused by the Gorkha earthquake and aftershocks appear to be far fewer than expected when compared with those of other mountainous regions with similar-magnitude earthquakes (31, 32). This might be due to the lack of surface ruptures induced by the earthquakes and the concentration of deformation along the subsurface thrust fault at 10 to 15 km depth (2).

Landslide distribution

Control by shaking and slope

The locations of the Gorkha earthquake-induced landslides are plotted with landscape physiography and the epicenters of the six largest shocks

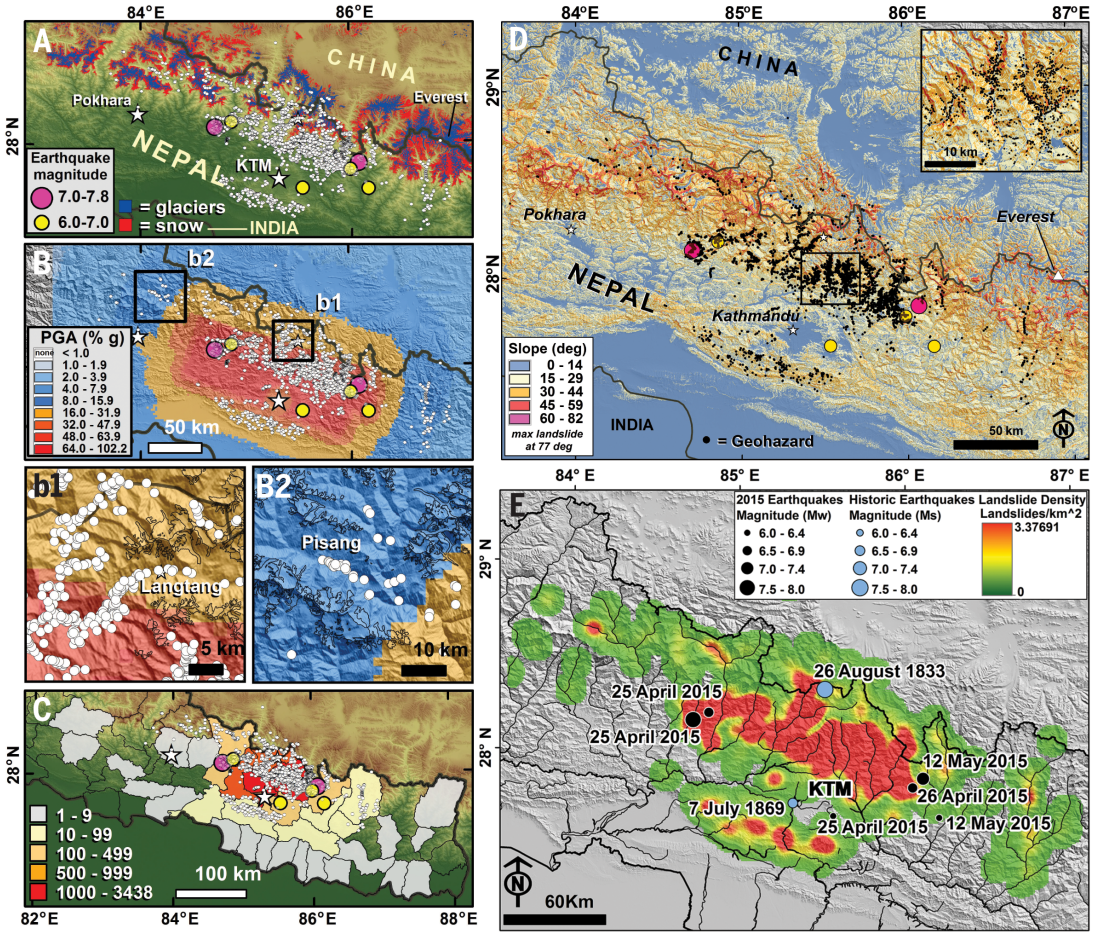

Fig. 1. Location of 4312 earthquake-related geohazards. (**A**) Distribution of glaciers (blue), late-season snowfields (red), landslides (white dots), and main shock and largest aftershock epicenters. The base topography is from the SRTM 90-m gap-filled digital elevation model (33). Glacier extents are from the Randolph Glacier Inventory (RGI) (61). Snowfields were derived from pre-event Landsat-8 visible and near-infrared (VNIR) to short-wave infrared (SWIR) band ratios and topographic masks. (**B**) (Top) Landslides plotted with local peak ground accelerations induced by the main Gorkha shock or M >6 aftershocks. PGAs are from the USGS–National Earthquake Information Center ShakeMap (62). (Bottom) Boxes b1 and b2 are enlarged to show details near Langtang and Pisang. (**C**) Landslides plotted with reported deaths per Nepal district are from the Government of Nepal, Nepal Disaster Risk Reduction Project. (**D**) Hazard occurrences (black dots) on calculated slopes. (Inset) Detail of hazard-dense region. (**E**) Smoothed area density (log scale) of earthquake-induced landslides determined by using a neighborhood 1/8° by 1/8° search window (~14 by 12 km) in relation to major (M ≥6) epicenters of historic earthquakes and the Gorkha quakes (62). Densities range between 0.01 and 3.37 landslides/km^2. Higher landslide densities occur locally on scales finer than 1/8°.

(Fig. 1A), PGA (Fig. 1B), reported deaths (Fig. 1C), and slope (Fig. 1D). We also mapped the smoothed landslide density distribution (Fig. 1E) and computed and mapped the susceptibilities of the landscape to earthquake-induced mass movements of ice, snow, or rock (Fig. 2). The computed susceptibilities depend on the product of the sine of slope (*33*) and the PGA (from the USGS ShakeMap PGA) (Fig. 1B).

Integration of slope and shaking (represented by PGA) within the susceptibility index partly accounts for where landslides occurred (Fig. 2), especially where collapse of high-elevation snow and ice may have been involved (Fig. 2, B and C). The landslide distribution shows the strongest associations with slopes of >30° (Fig. 1C and fig. S2A), PGA of >0.32*g* (Fig. 2A and fig. S2B), and shake-induced landslide susceptibility index of >0.16*g* (Fig. 2A). We infer that many of these landslides probably would not have occurred anytime soon without earthquake shaking. The control of landslide occurrences by the steep Himalayan slopes and seismic shaking is unsurprising and similar to other well-documented earthquakes (*34*). However, landslide susceptibilities differ from quake to quake. These new results detail the relationships of this Himalayan earthquake to seismic and geologic/terrain parameters. As PGA attains several tenths of *g*, entire mountainsides can collapse as shake-induced coseismic failures are not restricted to materials and terrains that were already poised near failure. Whereas landsliding on steep, strongly shaken slopes is easily understood, the tail of the landslide distribution to low shaking values, to low slopes, and low (but nonzero) shaking-induced landslide susceptibilities (fig. S2) requires further explanation.

Under any of the following conditions, low seismic PGAs at a few percent of *g* may cause failures that lead to a landslide or avalanche if the materials are already near failure.

(i) Granular materials may accumulate near the angle of repose, making them susceptible to coseismic failure owing to an acceleration that would increase shear stress along incipient planes of failure or related to rapid coseismic vibration-induced creep (*35*).

(ii) Seismic vibrations may cause liquefaction of water-saturated sediment, disturbances to the local hydrology, and coseismic or postseismic flow or rotational slumping (*36*).

(iii) At the beds of polythermal glaciers, the frictional resisting force may be carried by small frozen domains (*37*). Sharp accelerations may fracture the bed's frozen attachments, suddenly reducing the frictional force and initiating sliding.

(iv) Motion of rock or ice on fracture planes is resisted by the frictional force at the slip plane (*38*). Reduction in the normal stress because of downward acceleration, or increase in the downslope driving shear stress because of slip-plane parallel acceleration, may initiate coseismically triggered slip on steeply sloping slip planes.

(v) Upward acceleration increases the normal stress and may induce transient pressure melting of basal polythermal ice, reducing the frictional force. The subsequent downward seismic acceleration suddenly relieves the normal stress, so that newly produced basal meltwater (which might not refreeze) may initiate sliding (*39*).

The mechanisms outlined above may produce landslides or avalanches at low but nonzero shaking in granular materials occurring on steep slopes, in water-saturated sediments, and on steeply sloping glaciers. The deadly Mount Everest ice/snow avalanches on 25 April 2015 exemplify this point, where shaking was a low 0.09*g* (table S3). Glacier ice and snow are commonly poised near failure as indicated by Everest's history of ice avalanches off steep slopes, including back-to-back years in which there were a record 16 avalanche deaths in April 2014 (triggered by spring melting) and a new record 22 deaths in April 2015 (earthquake-triggered). Many Himalayan glaciers are substantially avalanche-fed, and snow or ice avalanches may occur upon a slight prompt, whether because of heavy winter or monsoon snowfall, spring melting, or slight shaking. The Gorkha earthquake struck soon after another season of spring melting began, increasing the vulnerability to shaking of ice and snow in the Everest area. Landslides in the upper Marsyangdi Valley (described below) also experienced relatively weak shaking (0.11 to 0.13*g*) but involved unconsolidated fluvial gravels and lacustrine silts (*40*).

Seismic reactivation of preseismic landslides, or hydrological reactivation of earthquake-triggered landslides, may be common where landsliding already is present. Hydrological reactivations may be caused by precipitation runoff, spring discharge, or erosional undercutting of river banks. Image time series indicate that many mapped landslides, such as in the Marsyangdi Valley, happened after the main shock. In general, these might be attributable to a host of factors such as aftershocks, failure of earthquake-disturbed hanging glaciers or debuttressed slopes (*41*, *42*), degradation of mountain permafrost and glacier-permafrost interactions (*41*), extreme precipitation, and stream undercutting of poorly consolidated sediment banks that were already disturbed by the earthquake. These mechanisms involve changes to the

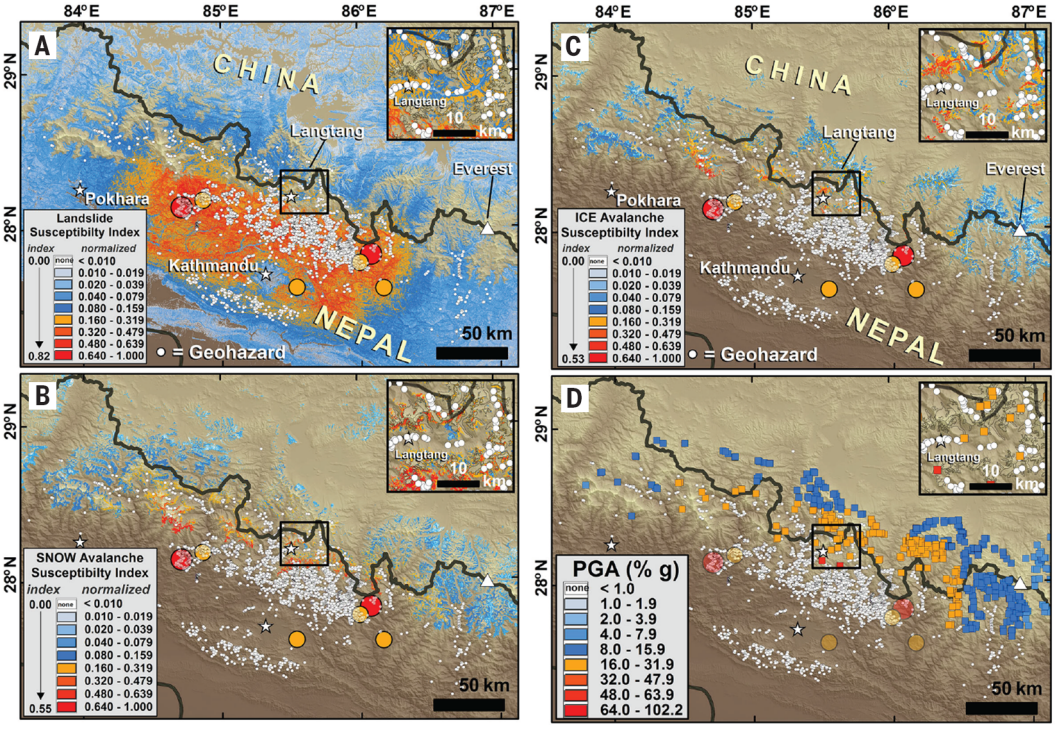

Fig. 2. Debris landslide susceptibility with mapped hazards. (**A**) Susceptibility in units of acceleration divided by *g* (9.81 m s^{-2}). (**B**) Snow avalanche susceptibility with mapped hazards. Susceptibility is in *g*. (**C**) Ice avalanche susceptibility with mapped hazards. Susceptibility is in *g*. (**D**) Maximum PGA experienced by 491 glacier lakes. Mapped hazards are shown as white dots. Maximum PGA for glacier lakes was 0.57*g*. (Insets) Detail in Langtang Valley.

supply of groundwater or rates of glacial erosion or ice melt, which have at least indirect links to climate change.

Control by the broad-field seismic deformation

Another key earthquake phenomenon is the wide-field land surface deformation pattern, which appears to have influenced the distribution of landslides (Fig. 3). The mapped surface deformation was derived from Interferometric Synthetic Aperture Radar (InSAR) (Fig. 3A) (*43*). While the ALOS-2 InSAR measurement is in the radar line-of-sight, GPS measurements show that the horizontal motion is almost in the along-track direction, so the InSAR displacements in Fig. 3A are almost purely vertical (*3*). The highest densities of landslides are correlated with the down-dropped block, which is on the back-limb of the hanging wall of the thrust and counterintuitively correlates with the higher Himalaya. Within this block, landslide densities increase southward and then abruptly decrease near the tectonic hinge line, which separates the downdropped and upthrown blocks (and also approximates the zone of maximum slip on the fault). RADARSAT-2 data provide the horizontal displacement field over part of the earthquake-affected region and confirm that the largest horizontal displacements (Fig. 3B) are near the hinge line and in the uplifted block, as defined by vertical deformation (Fig. 3A).

We do not fully understand the distinctive concentration of earthquake-induced landslides in the tectonic downdropped block of the Gorkha earthquake. The steep slopes within the downdropped block no doubt contributed to the pattern of landslide densities, but steep slopes are also present in some areas where landslides are few. The net downward acceleration implied by the downdrop possibly caused a momentary reduction in lithostatic stress, hence a reduction of normal stress along inclined planes of weakness. Relief of normal stress could have allowed non-lithostatic shear stress, including lateral seismic acceleration, to initiate motion along landslide failure planes. Because the coefficient of sliding friction is normally less than that of static friction, motion may then continue and drive a landslide. The same mechanism may apply to shaking, and hence, the broad-field deformation may modulate the shaking-induced perturbation of normal stress, again suggesting some integration of multiple causative trigger mechanisms.

The Gorkha earthquake caused fewer landslides than expected on the basis of its magnitude (*12*, *32*), mirroring the unexpected paucity of dwelling destruction (*2*). The peculiar distribution of the Gorkha earthquake landslides on the downdropped block (Fig. 3) placed them mainly north of the major population centers, reducing the death toll. For strike-slip events such as the 2010 M 7.0 Haiti earthquake (*44*), landslides were not similarly distributed systematically with respect to the fault plane. For comparison, landslides in the 1994 M 6.7 Northridge and 2008 M 7.9 Wenchuan earthquakes (*11*, *12*, *45*) were concentrated on the higher mountainous areas of the upthrown block. Both earthquakes were oblique thrust events, like the Gorkha quake. The Wenchuan earthquake induced far more landslides than did the Gorkha earthquake, despite similar steep terrain. These differences might relate to the Gorkha quake's shallow dipping fault and lack of surface rupture (a blind thrust).

The Northridge earthquake was also a blind thrust, and despite being smaller than the Gorkha quake, it produced 11,000 documented landslides (*45*). Some, mapped by an airborne survey, were smaller than the detection limit in the imagery used for our survey, in which Digital Globe data were unavailable. The numerous slides caused by the Northridge earthquake may be primarily attributed to uncemented clastic sedimentary compositions dominating the regional lithology, versus more competent high-grade metamorphic and igneous rocks dominating the higher Himalaya. The differing types and densities of vegetation and root binding might also be a factor. In general, differences in earthquake-induced landslide densities can also be related to the number and magnitude of strong high-frequency ground motions, although the paucity of strong-motion

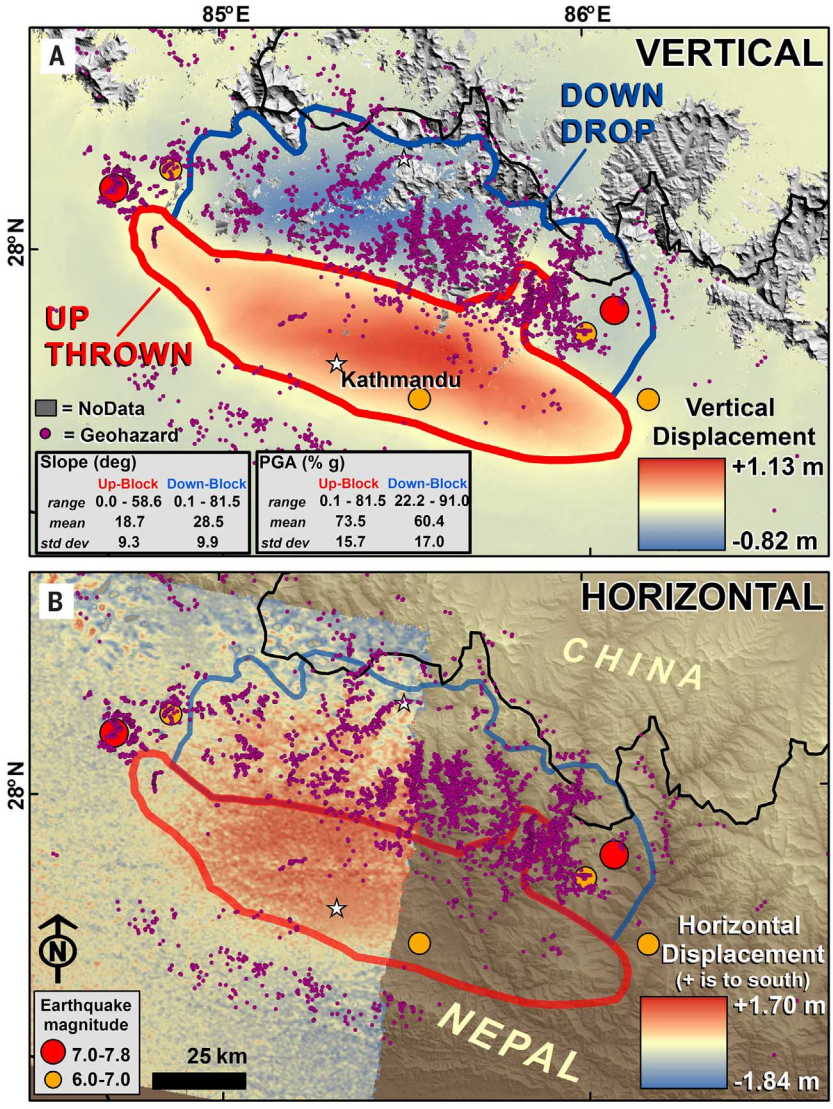

Fig. 3. Landslide distribution relative to the Earth surface deformation field. (**A**) 4312 landslides (purple dots) are concentrated mostly north of the hinge line between the downdropped block and uplifted block. Also shown are the epicenters of the main shock and five largest aftershocks. Vertical displacements are from the JAXA ALOS-2 ScanSAR interferogram (21 Feb and 2 May 2015 scenes), which represent almost entirely vertical motion. ALOS-2 interferometry of the Gorkha earthquake and largest aftershock was recently described by Lindsey *et al*. (*3*). (**B**) Horizontal motion map based on azimuth shift measurements of the RADARSAT-2 XF acquisitions of 5 April and 29 April 2015. Scale shows motion excluding outliers outside the mean ± 3σ. Values are positive for SSW azimuths >100 degrees relative to east (>S10W). Hence, both the upthrown and downdropped blocks shifted southward. The areal coverage for the RADARSAT-2 scene is not identical to that of ALOS-2; areas on the eastern side of the scene have no data.

recordings in the cases of both the Gorkha and Wenchuan quakes hampers direct comparison.

Control by lithology and major fault structure

The local clustering indicates additional controls on landslide occurrence. Lithologic variations, sediment thickness, bedding dip direction relative to slope aspect, extent of physical and chemical weathering including extent of bedrock fracturing, and vegetation cover may be important controlling factors. Lithology affects the occurrence of some landslides. For instance, the Langtang Valley slides involved the failure or ingestion of ice and unconsolidated glacial debris. Another example is the poorly consolidated sediment driving the Marsyangdi Valley landslides.

Fault structures exert indirect control of the clustering of landslides and organization of clusters (Fig. 4). High concentrations of landslides occur within particular Proterozoic metamorphic units and intrusive complexes and also near the surface of several major tectonic features, mainly low-angle thrust faults including the South Tibetan Detachment System (STDS), the Main Central Thrust (MCT), the Main Boundary Thrust (MBT), and the Main Frontal Thrust (MFT). The latter three faults splay off the subsurface Main Himalayan Thrust, which is thought to have slipped during these earthquakes (*1*). However, because none of the Gorkha earthquake fault displacements (main shock or aftershocks) are known to have pierced the surface, the association with the thrust faults might indicate underlying lithological control, in which the faults juxtapose rocks of differing compositions at the surface. Lithologic properties influenced the topographic character of the landscape and how seismic energy is transmitted, particularly through (i) elastic and brittle/elastic properties of the rock, (ii) chemical weathering and its control of erosion and slope, (iii) fracture development and fault displacement, and (iv) seismic wave interactions with topography and lithological structures. Each factor likely contributes, where lithology is a common denominator. A high density of landslides occurs within the upper Lesser Himalaya near to and east from the epicenter of the primary earthquake. Whereas this cluster's proximity to the largest shock's epicenter is evident, the pattern defined by the cluster is closely correlated with the outcrop of the upper Lesser Himalaya, which is composed of low- to medium-grade metamorphosed Proterozoic argillic-calcareous (clay and sand) units and also of higher-grade metamorphic Proterozoic rocks. The upper Lesser Himalaya here is bounded on the north by the Main Central Thrust, where the overthrusted rocks are dominated by Precambrian gneisses, but only near the thrusted contact do the latter underlie many landslides.

Many landslides occur south and west of Kathmandu (Fig. 4) near the southern edge of the Kathmandu Nappe [a thrust sheet of Precambrian/Lower Paleozoic metasedimentary rocks, as mapped by Stöcklin (*46*)]. In these areas, landslides are especially concentrated where Ordovician granitoids have intruded Proterozoic metasediments, suggesting lithological contrast as a controlling feature. Further, there is a notable absence of landslides south of the MBT-MCT south of Kathmandu.

Proterozoic slate, shale, siltstone, sandstone, graphitic schist (Fig. 4, combined as purple) and gneiss (Fig. 4, red)—all layered rock types—host relatively few landslides. Instead, the vast majority of earthquake-triggered landslides occur in the Proterozoic phyllite, amphibolite, metasandstone, and schist rock sequences of the Lesser and High Himalaya (Fig. 4, green and pink) north of Kathmandu. These occur on either side of the MCT. The landslide hotspots (Fig. 1E) comprise a small fraction of the area of this widespread rock unit; steep-sided, high-elevation ridgetops generated some of the landslide hotspots. For example, the Langtang Valley landslides largely originated high on the ridges and near the summits in places where glaciers, glacial debris, and bedrock failed. The lithological controls may manifest through rock mechanics and rock weathering and slope.

Topographic effects, along with different rock types' contrasting *S*, *P*, and surface waves affect landsliding through wave scattering, interference, and heterogeneous energy dissipation. During helicopter overflights, authors B. Collins and R. Jibson (*47*) observed pervasive ridgetop shattering through much of the near-epicentral landsliding region. Constructive wave interference and the focusing of seismic energy to shatter ridgetops was observed in the Northridge (*48*) and 1971 San Fernando (*49*) earthquakes and modeled for the 2005 I-Lan earthquake in Taiwan (*50*). Last, damage related to wave resonance occurred in the Kathmandu Basin during the Gorkha earthquake (*2*), and similar resonant effects may have occurred elsewhere at damaging frequencies affected by the spatial scales and geometry of various lithologic units. Human-built structures of different sizes and construction, having distinctive resonant vibrational frequencies, were selectively destroyed (*2*).

Some major river valleys also have high landslide densities, including along the Marsyangdi and Trishuli rivers. In the Marsyangdi Valley, a high landslide density correlates with relatively gently sloping areas of the valley floor that are covered by poorly consolidated sedimentary deposits.

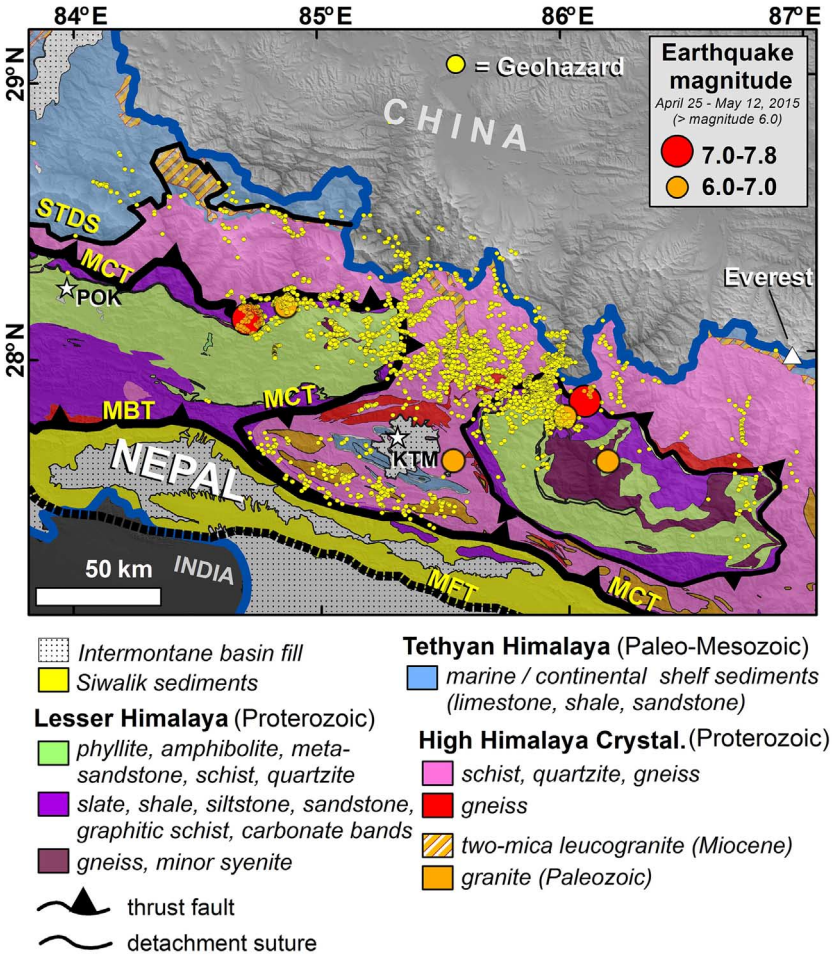

Fig. 4. Landslide occurrence on mapped geologic units. Geology is from simplified geologic map by (*46*, *63*) and major faults (*64*).

Langtang mass movements

The earthquake-induced landslides of the Langtang Valley (Fig. 5 and figs. S3 to S6) were exceptional

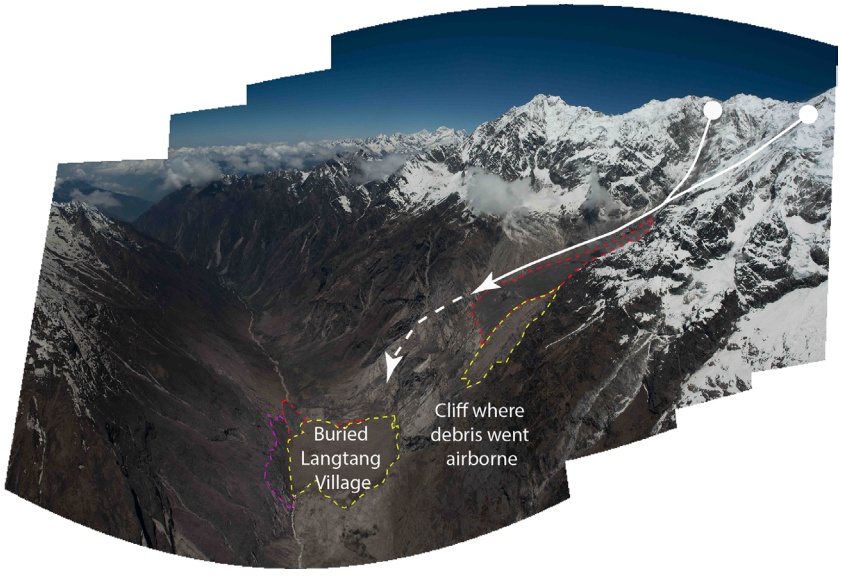

Fig. 5. Langtang's landslide flowpaths. The source areas and flow paths of the two Langtang mass movements (white arrow, dashed where airborne). The red dashed line indicates the extent of the first slide, the yellow dashed line indicates extent of second slide, and the purple dashed line indicates extent of debris run-up. The image is west-facing. [Stitched panorama from 10 May 2015; photos by D. F. Breashears/GlacierWorks]

in their tragic results (more than 350 people killed) and are also among the Gorkha earthquake's best-documented landslides from field- and space-based analysis. Langtang Valley, 70 km north of Kathmandu, is one of Nepal's major trekking regions and hosts benchmark glaciology, hydrology, and meteorology research (*51*–*53*). The valley experienced moderate shaking (up to ~0.26*g* above Langtang village) (Fig. 1B). An analysis of post-event satellite imagery and oblique aerial photographs suggests that coseismic snow and ice avalanches and rockfalls and their powerful concurrent air blasts contributed to the destruction in Langtang Valley (Fig. 5 and figs. S3 to S6) that killed or left missing at least 350 people (*54*). Panoramic photos of Langtang taken in 2012 and those taken after the earthquake on 12 May 2015 illustrate the magnitude and destruction of the Langtang events (figs. S3 and S4). Further indicating the vast scale of these events, annotated helicopter-borne photos and satellite imagery taken of the valley (Fig. 5 and figs. S5 and S6) illustrate our interpretation of this disaster-within-a-disaster.

Debris from the initial coseismic event covered 7.51×10^5 m^2 at Langtang alone, including a ~1-km stretch of the Langtang River. We did not observe stream impoundment in the days after the earthquake, indicating that meltwater and runoff tunneled rapidly through the icy deposit. Photos (D. Breashears) showed that the deposit contained abundant snow and ice. Brightness temperatures modeled from thermal band 10 of Landsat 8 on 30 April 2015 showed lower landslide surface temperatures (270 to 280 K) as compared with those of surrounding terrain (280 to 300 K). The temperature anomalies, pond formation, and moisture of debris resulted from melting.

The primary coseismic event at Langtang village was a combined ice-snow avalanche that initiated near 7000 m. Subsequently, ice and snow entrained rockfall material and descended a low-gradient part of the glacier down to ~4500 m. The rock-ice mass then became airborne as it fell off a cliff below 4500 m (Fig. 5). After the material reached the riverbed at ~3250 m, it ran up the opposing slope ~200 m (fig. S5). The air blasts propagated farther, 400 m up the mountain (fig. S3). From the impact point on the valley floor, devastation extended ~1 km up- and downvalley. From the 200-m-high surge of debris on the opposing slope, we estimate a debris speed (v) of 63 m s^{-1} (227 km h^{-1}) following Eq. 1

$$v = (2gh)^{0.5} \quad (1)$$

where g is gravitational acceleration (9.8 m s^{-2}) and h is the runup. Air blasts leveled what was not buried in Langtang, including some buildings constructed of stone slab. Wind also completely flattened a small forest, suggesting wind speeds comparable with an EF5 tornado (>322 km hour^{-1} wind speed), which is consistent with freefall drop of the landslide and heavily debris-laden wind over the cliff.

Satellite images provided by Digital Globe (fig. S6) indicate a second large post–main shock mass movement near Langtang village between 8 and 10 May 2015. The source of this landslide may have been a rock detachment from the summit ridge of Langtang-Lirung, ~6700 m elevation. The second landslide slightly increased the debris area from 7.51×10^5 to 7.61×10^5 m^2.

Nearby settlements of Singdum and Mundu (fig. S6) were also damaged by air blasts from the Langtang Valley mass movements. The larger settlement of Kyangjin was also badly damaged by an air blast created by another avalanche that originated from the eastern ridge of Langtang-Lirung. Devastation in the air-blasted zones, as captured in several photos (fig. S3), is indicative of the huge energy involved. The first Langtang landslide mass may be ~3.3×10^9 kg (area ~750,000 m^2, assumed mean thickness ≥2 m, density 2200 kg m^{-3}). With a direct fall of ~1 km, the release of gravitational potential energy was ≥3.2×10^{13} J (7.6-kiloton TNT equivalent). During freefall and impact, the main transfer of energy could only have been to the atmosphere and directly on the surface, the effects of which we sadly observed.

Landslide blockages of rivers: Marsyangdi and Tom rivers (Nepal) and Gyirong Zangbo/Trishuli River (Tibet)

We identified recurrent landslides along the upper Marsyangdi River in the Annapurna region. These are a different type of landslide than those in Langtang Valley. At least 20 mass movements intersected the river in the 10 days after the main shock (Fig. 6). The rapid sequence of similar failures demonstrates that the quakes in some way disturbed the unconsolidated sediments (*40*) along the river, perhaps by altering the hydrology or opening soft-sediment fractures, which then were exploited by spring seepage and erosion and rotational failures.

The Marsyangdi Valley experienced relatively weak shaking (to ~0.13*g*) (Fig. 1B and table S3), which triggered nine small landslides along a 16-km stretch of the upper Marsyangdi River between Humde and Bratang (Fig. 6). The landslides were identified from a WorldView-2 satellite image 27 April 2015, 2 days after the earthquake, but were not present in a Landsat 8 image 4 days prequake. Thus, we considered them primary effects of the main shock. Some slumps constricted but did not greatly obstruct the river. One landslide (Fig. 6), ~2.2 km upstream of Lower Pisang village, caused a small impoundment (135 m long, ~2×10^3 m^2).

Five more landslides reached the river between 27 April and 2 May 2015, including one ~200 m wide, which caused a complete blockage ~1.9 km upstream of Lower Pisang. The impoundment grew to ~550 m long and 30 to 40 m wide (~1.4×10^4 m^2) (Fig. 6). Six new landslides occurred by 4 May, and the lake increased to ~2.5×10^4 m^2 and 1100 m long, the same as measured again on 28 May 2015. Upstream, several smaller impoundments indicated a further hazardous situation in which a dam breach could initiate a succession of lower dam breaches and the inundation of Lower Pisang village.

Ground photographs (Fig. 6B) show a predominantly fine-grained landslide (*47*), likely composed of fluvial and lacustrine sediments from former dammed lakes (*40*). The steep headwall, back-tilted trees, and a sharp detachment at the head of the landslide indicate that the slide is a rotational slump, a common failure mode in poorly supported, unconsolidated sediments.

The appearance of eleven post–main shock landslides and growth of the impoundment lake represent secondary and tertiary effects of the earthquake and indicate that the region is susceptible to long-term slope instability and future landslides.

We observed many other earthquake-induced landslide blockages of rivers. In one case, a 450-m-wide landslide blocked the lower Tom River near Ghap, Manaslu Conservation Area, Nepal, creating an impoundment lake that stirred urgent humanitarian concerns. Satellite imagery from 3, 5, 7, and 8 May has allowed monitoring of the dammed lake. Between 3 and 8 May, the lake grew from ~5.7×10^4 to ~6.6×10^4 m^2. The nearby village of Ghap, located downstream of the confluence of the Tom and Budhi Gandaki rivers, fortunately showed no flood damage by 16 May, indicating that even though the lake was draining through a narrow outlet, the dam erosion was gradual. A satellite image from 8 June and subsequent media coverage shows that most of the lake had drained without severe consequences.

The Gorkha earthquake and its many aftershocks also triggered dozens of landslides into the south-flowing Gyirong River, China (Trishuli River downstream in Nepal). One landslide dammed the river ~1.5 km south of Chongsecun, a few kilometers north of the Nepalese border, causing development of a 450 by 50 m impoundment lake (28.363N, 85.360E, ~2600 m above sea level). The landslide destroyed ~200 m of the road connecting Chongsecun to the China-Nepal border crossing at Resuo. Boulders and debris were displaced downslope, forming a landslide scar ~700 m long and a deposit 250 by 300 m. Several landslides and a landslide-dammed lake also developed south of the Chongsecun slide at or near the Resuo border crossing in Nepal (28.275N, 85.379E, ~1,810 m above sea level) and blocked the road near the Resuo bridge. Fortunately, the dam was incised by the river, and with mitigation efforts by engineers, there was no further damage. Another landslide on the same river near Resuo was triggered by a rainstorm on 28 April 2015, with the terrain conditioned by the M 7.8 Gorkha earthquake. The landslide dammed the Trishuli River and blocked the road from Gyirong County to Resuo Port. These features near Chongsecun and Resuo exemplify the transboundary process chains of some induced hazards. The interruption of cross-border commerce is a major tangible earthquake impact in addition to the damage to infrastructure and the loss of life.

Glacier lakes stability

Many GLOFs have been recorded in the Himalaya since the mid-20th century (*55*). The lakes' moraine dams, commonly situated at the angle of repose, are fragile and prone to outburst because of either sudden collapse or piping erosion, or to gradual degradation due to climatic warming and thaw. Avalanche and landslide-generated displacement waves in the lake are thought to be a common trigger for moraine dam failure (*56*). Thus, when the largest earthquakes happened,

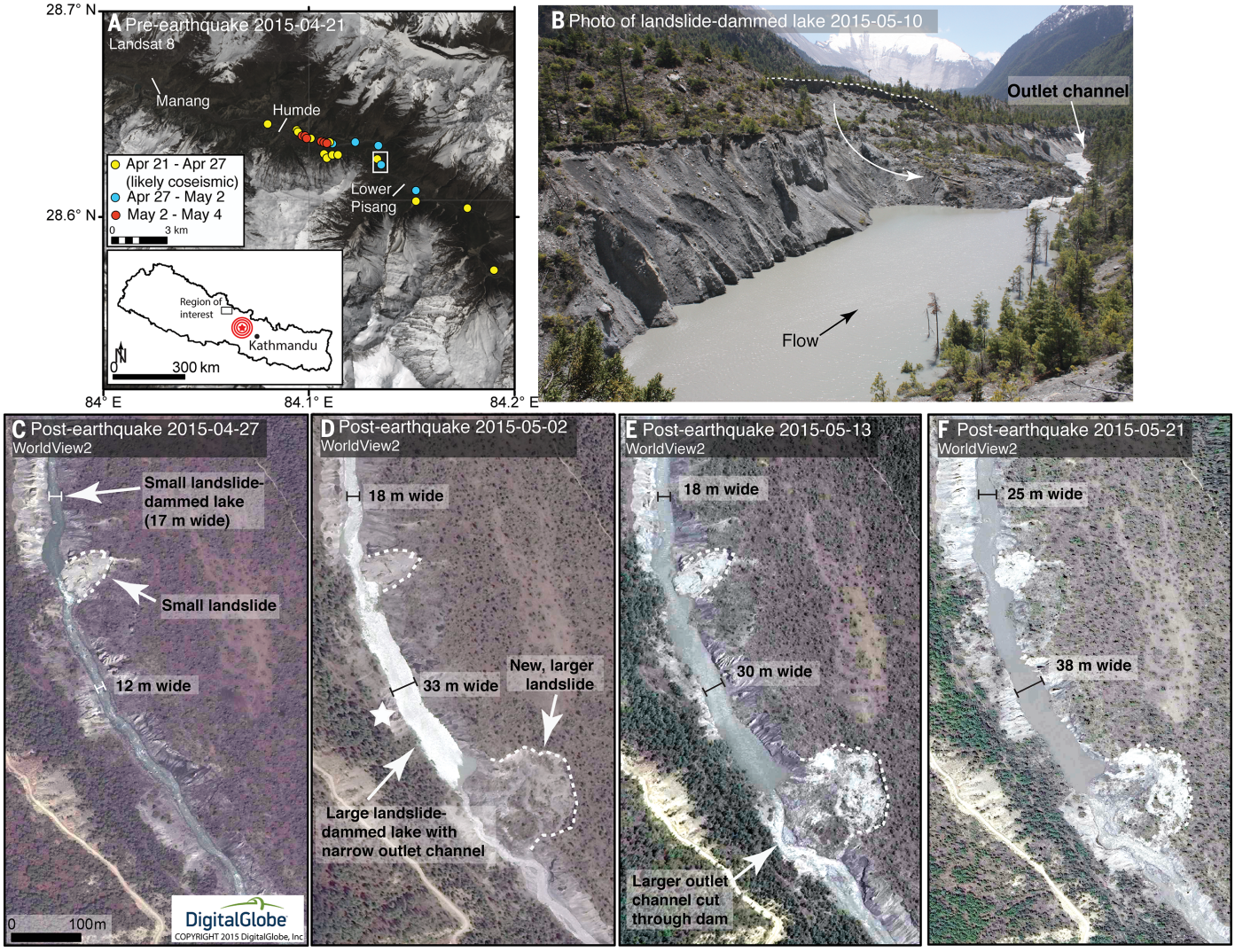

Fig. 6. Landslide-dammed lake on the Marsyangdi River. Map and satellite imagery and ground photographs of landslides and landslide-dammed lakes on upper Marsyangdi River. (**A**) Map. White box locates (C), (D), (E), and (F). (**B**) Ground photograph (courtesy M. Gotame, Manang villager) from 10 May 2015, showing the landslide-dammed lake looking south. The white dashed line is the head scarp (visible is the steep headwall), and the curved arrow shows the inferred flow path of the rotational slump. (**C**, **D**, **E**, and **F**) High-resolution WorldView-2 images of the river, showing delayed occurrence of the large landslide and lake formation. The white star in (D) locates (B). River widths are given at two locations.

many experts were concerned that shaking may have weakened or collapsed unconsolidated moraine dams of glacial lakes, or may have triggered large displacement waves and GLOFs.

Fortunately, we identified few earthquake effects on glacier lakes. We examined pre- and postquake satellite images of 491 lakes [locations drawn mainly from the inventory of Fujita *et al.* (*57*)]. The visibility of 15 lakes in our database was unclear (partially shadowed or poor resolution image), but their downstream drainages showed no signs of GLOFs. Only nine of 491 were physically hit by landslides or avalanches. Of these, ice avalanches may have ejected water from two small ponds near Everest, and debris fell onto the frozen surfaces of other lakes without further effect. No lakes in the current satellite survey produced a GLOF as a result of the earthquake. GLOFs generally do not trigger at modeled PGAs up to 0.57*g* (Fig. 2D). This unexpected result may relate to seismic wave interactions with the topography, where for shallow hypocenters, PGAs (i) are reduced on valley floors and (ii) are rapidly reduced by shielding across mountain ranges caused by wave scattering on the topography and petrologic structure (*50*, *58*).

Furthermore, we closely examined three large moraine-dammed glacial lakes (Thulagi, Rolpa, and Imja) (Fig. 7), which have been extensively surveyed, studied, and monitored because of their GLOF risk (*55*). At Thulagi Lake in the Manaslu region (just west of the Tom River blockage described above) and Imja Lake in the Everest region, no damage was immediately evident in postquake satellite imagery. However, a small glacial lake on Lhotse Glacier (south of Everest) drained on 25 May 2015, which resulted in an anomalous rise in stream level (*59*). Small supraglacial ponds commonly drain suddenly because of ice fracturing or other glacier dynamics, and it is unclear whether this event was earthquake-related.

We were especially concerned about Tsho Rolpa, located at the terminus of Trakarding Glacier in the Rolwaling Valley, because of its location near the giant aftershock's (*M* 7.3 on 12 May) epicenter. We found no evidence of damage to Tsho Rolpa's damming moraine from examination of WorldView 1 satellite images taken 9 days after the initial earthquake, on 4 May 2015, and the NASA's EO-1 satellite image taken 5 days after the *M* 7.3 aftershock on 17 May. Postquake field photographs taken by USGS on 27 May show that the moraine was intact, and the lake was nearly brim-full (Fig. 8A). Another USGS photograph (Fig. 8B) shows fractures on the moraine dam, but because no ice exists in this part of the moraine, these tension cracks appear to have been caused by slumping of moraine material toward the lake (1 to 1.5 m horizontal and ~0.5 m vertical), probably because of an earthquake but not likely to be a problem. The satellite imagery and field photographs do not demonstrate any big new additional concerns about the lake. We would not observe small GLOFs and minor damage to moraines in satellite images because of limitations in resolution. Furthermore, neither satellite and ground nor helicopter-borne inspections can easily detect interior (subsurface) structural damage that make the metastable lakes even more subject to outburst.

Summary and conclusions

Rapid, systematic mapping allowed us to investigate earthquake-induced geohazard processes and provide information to relief and recovery officials on the same timeframe as those operations were occurring. This work thus contributed to effective, timely guidance to in-country authorities responsible for response and recovery. Key findings were relayed through NASA, USGS, and the U.S. Agency for International Development (USAID), to Nepal-based experts at ICIMOD (International Centre for Integrated Mountain Development) and DHM (Department of Hydrology and Meteorology, Government of Nepal) and to the Prime Minister of Nepal.

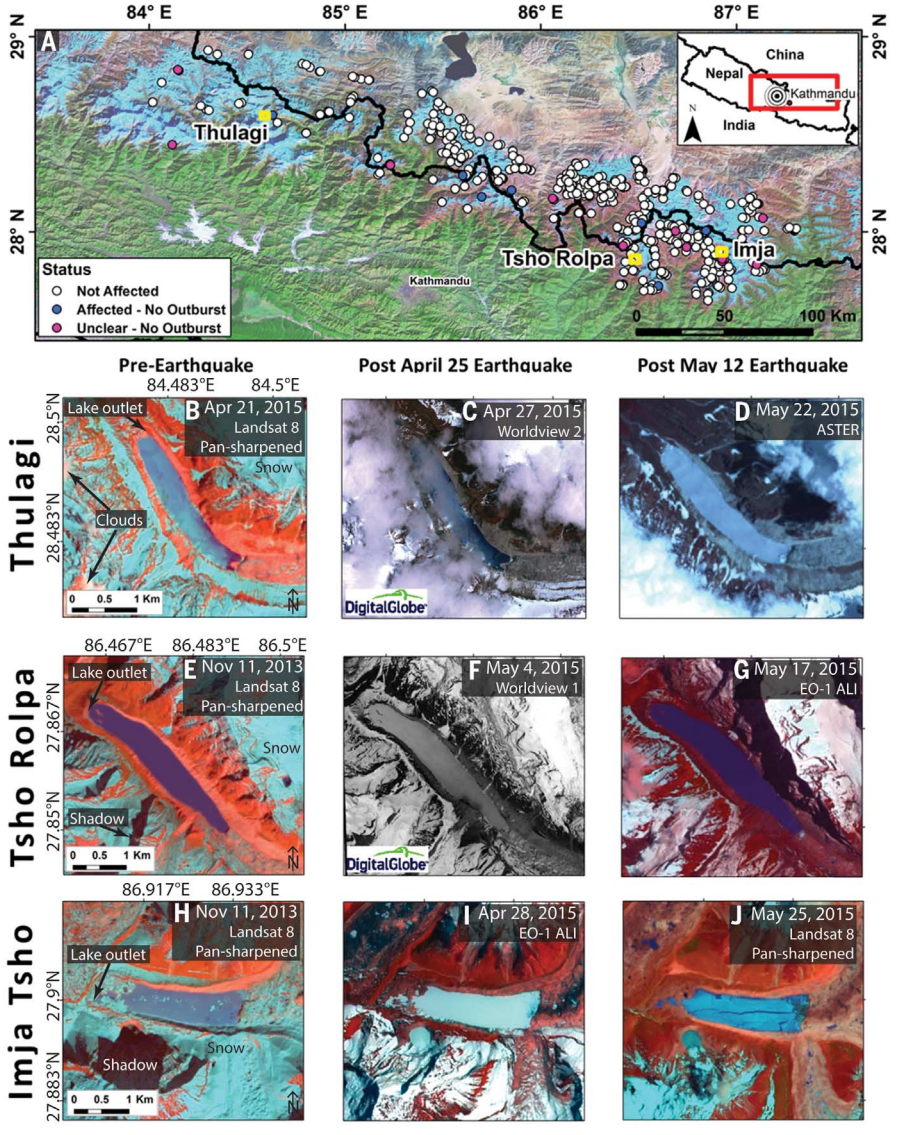

Fig. 7. Lake survey for earthquake damage. (**A**) Overview of study area, showing location of 491 surveyed lakes. (**B** to **J**) Pre-earthquake images (right column), post–main shock images (center column), and post–12 May aftershock images (left column) for the largest glacial lakes in Nepal, (B) to (D), Thulagi Lake, (E) to (G) Tsho (Lake) Rolpa, and (H) to (J) Imja Tsho. (B) Landsat 8 image of Thulagi Lake, 21 April 2015. (C) Worldview 2 image of Thulagi Lake, 27 April 2015. (D) ASTER image of Thulagi Lake, 22 May 2015. (E) Landsat 8 image of Tsho Rolpa, 11 November 2013. (F) Worldview 1 image of Tsho Rolpa, 4 May 2015. (G) EO-1 ALI image of Tsho Rolpa 17 May 2015. (H) Landsat 8 image of Imja Tsho, 11 November 2013. (I) EO-1 ALI image of Imja Tsho, 28 April 2015. (J) Landsat 8 image of Imja Tsho, 25 May 2015. A large crack developed in the lake ice on Imja Tsho, although such cracks are normal with spring thaw. Landsat 8 scenes are panchromatic band 8 sharpened images (resolution 15 m) using band combinations [7,5,3] (SWIR, NIR, Green). WorldView 2 false color composite scene uses band combination [7, 5, 3] (NIR, Red, Green). WorldView 1 image is the panchromatic band. ASTER image (resolution 15 m) uses bands [3N, 2, 1] (NIR, Red, Green). EO-1 ALI scenes use pan-sharpened band 1 (resolution 10 m) and band combination [8, 6, 4] (SWIR, NIR, Green).

The mapped features document the large geographic extent of the Gorkha earthquake's effect on hazardous Earth surface processes and constrain their geophysical limits and geomorphic, tectonic, and lithologic controls. The distribution of induced landslides shows positive associations with slope and shaking intensity. More broadly, the highest areal densities of landslides are developed primarily on the downdropped northern tectonic block. This is likely explained by momentary reduction during downward acceleration of the normal stress along planes of weakness. The largest two shocks bracket the landslide distribution because they are within the displacement field and highest PGAs. Additional controls of landslide distribution are indicated by their clustering within specific bedrock and surficial lithologies, including Proterozoic metamorphic rocks and Ordovician granitoids, in proximity to earthquake epicenters, with high PGAs, and perhaps with seismic wave scattering and interferences.

In the remote valleys of the higher Himalaya, the most concentrated losses were directly due to the induced mass movements and air blasts rather than shaking. Seismic wave interactions may have contributed to destruction in Langtang Valley and other locations because of wave focusing and ridgetop shattering but may have reduced direct shaking damage in valley floors and at glacial lakes.

The distribution of Gorkha earthquake–related landslides and the terrain susceptibilities to earthquake-induced mass movements provide a basis from which to predict future patterns of landsliding of earthquake-weakened ice, rock, and unconsolidated sediments, especially as aftershocks, precipitation, and snowmelt events continue over the next few years. Hydrological processes such as frost shattering and rockfalls at high elevations and riverbank undercutting and rotational slumping in valleys may exploit earthquake-induced damage and trigger more landslides. Conversely, high-magnitude shaking-related landslides, such as ridgetop failures that affected Langtang Valley, may be less common going forward, unless additional strong aftershocks or high-elevation melting affect seismically shattered rocks. However, earthquake-related landsliding may fade below the regional background frequency of landslide activity in the next one to several years.

The Gorkha earthquake caused fewer landslides than comparable earthquakes elsewhere, although some of Nepal's largest mass movements in recent millennia may have been triggered by earthquakes (*60*). Details of earthquake location relative to geology and topographic relief appear to be crucial in determining the magnitude of earthquake-induced hazards.

Although the Gorkha earthquake's tragic toll on human lives and culture cannot be understated, some fortunate facts are that not a single large GLOF was unleashed and the total number of landslides was far fewer than generated by comparable earthquakes (*56*). Whether the same will hold for a hypothetical future large Himalayan earthquake is uncertain. However, future earthquakes generated on the shallow Main Himalayan Thrust are not apt to generate many or any GLOFs unless the magnitude is greater than the Gorkha earthquake's or the hypocenter and zone of maximum slip is closer to the lakes, thus circumventing the shielding by Himalayan relief. The potential exists for immense landslides and river blockages, which may pose the greatest mountain hazard.

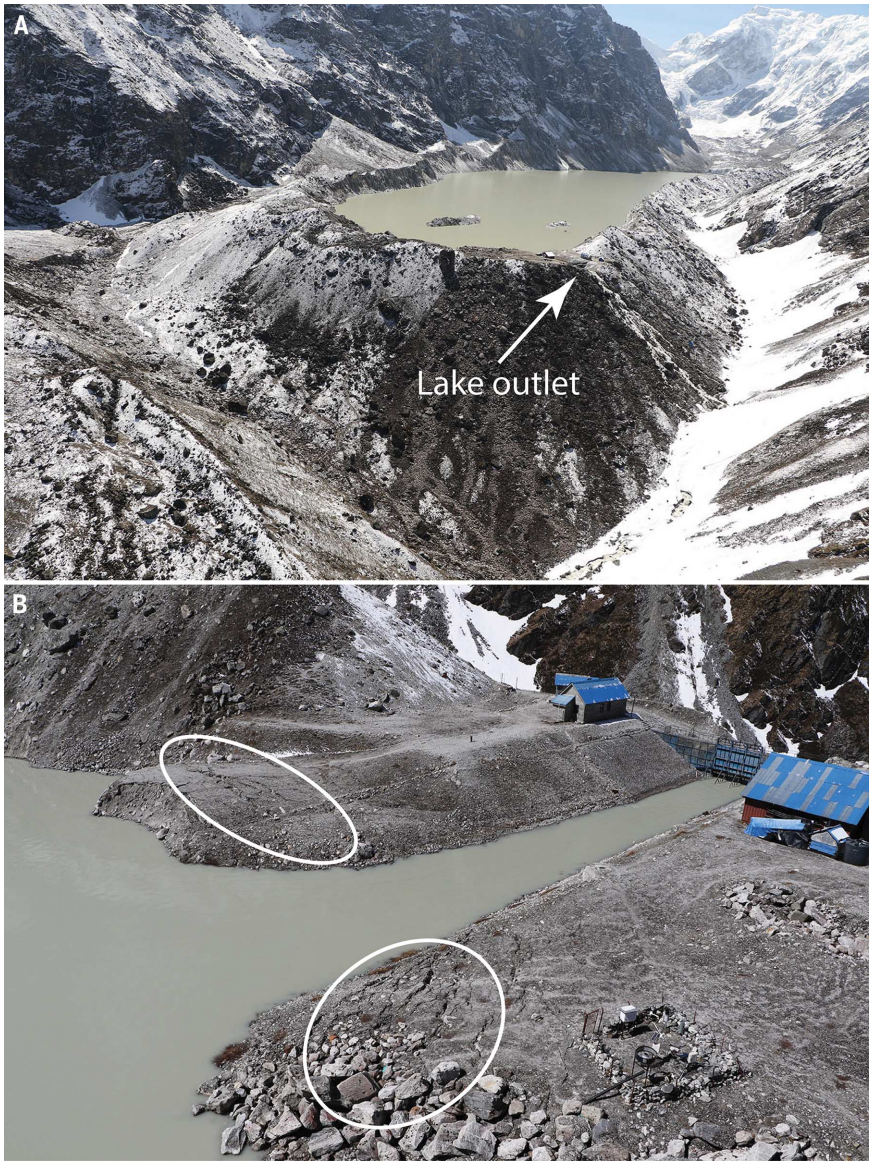

Fig. 8. Field visit identifies light damage at Tsho (lake) Rolpa. (**A**) Post-earthquake image of Tsho Rolpa appears identical to its appearance shortly before the earthquake. (**B**) Two areas of fractures (outlined in white)—believed formed by the 12 May 2015 aftershock—were observed from a helicopter on the engineered part of the end moraine during an inspection undertaken by USGS at Tsho Rolpa. Photos are from 27 May by B. Collins (USGS), courtesy of USAID–Office of Foreign Disaster Aid.

Materials and methods

We mapped 4312 landslides from high- and medium-resolution satellite imagery (Landsat 8, WorldView, and others) in the weeks after the *M* 7.8 main shock. Landslide locations were mapped as points, with attributes including nearest village, dates of imagery used to constrain timing, and whether the mass movement produced or could produce a secondary hazard (for example, a dammed lake). Using a previously published database and the multispectral satellite data, we also assessed damages to glacial lakes. The distribution of landslides was examined in the context of the geology (structure and lithology), the distribution of snow and ice, topographic slopes, and peak ground accelerations modeled for the Gorkha earthquake and its largest aftershock. Seismic and shake intensity data combined with slope were used to model geohazard susceptibility indices. All data, including previously published InSAR-measured ground displacements, were analyzed within a geographic information system.

REFERENCES AND NOTES

1. R. M. Parameswaran *et al*., Seismotectonics of the April–May 2015 Nepal earthquakes: An assessment based on the aftershock patterns, surface effects and deformational characteristics. *J. Asian Earth Sci.* **111**, 161–174 (2015). doi: 10.1016/j.jseaes.2015.07.030
2. J. Galetzka *et al*., Slip pulse and resonance of the Kathmandu basin during the 2015 Gorkha earthquake, Nepal. *Science* **349**, 1091–1095 (2015). doi: 10.1126/science.aac6383; pmid: 26249228
3. E. O. Lindsey *et al*., Line-of-sight displacement from ALOS-2 interferometry: M_w7.8 Gorkha Earthquake and M_w 7.3 aftershock. *Geophys. Res. Lett.* **42**, 6655–6661 (2015). doi: 10.1002/2015GL065385
4. K. Jaiswal, D. Wald, D. D'Ayala, Developing empirical collapse fragility functions for global building types. *Earthq. Spectra* **27**, 775–795 (2011). doi: 10.1193/1.3606398
5. J. S. Kargel, G. J. Leonard, M. P. Bishop, A. Kääb, B. H. Raup, *Global Land Ice Measurements from Space* (Springer-Verlag, Berlin Heidelberg, 2014).
6. E. L. Harp, D. K. Keefer, H. P. Sato, H. Yagi, Landslide inventories: The essential part of seismic landslide hazard analyses. *Eng. Geol.* **122**, 9–21 (2011). doi: 10.1016/j.enggeo.2010.06.013
7. J. A. N. van Aardt *et al*., Geospatial disaster response during the Haiti earthquake: A case study spanning airborne deployment, data collection, transfer, processing, and dissemination. *Photogramm. Eng. Remote Sensing* **77**, 943–952 (2011).
8. G. Cecchine *et al*., "The U.S. Military Response to the 2010 Haita Earthquake - Considerations for Army Leaders" (RAND Corporation, 2013).
9. H. P. Sato, E. L. Harp, Interpretation of earthquake-induced landslides triggered by the 12 May 2008, *M*7.9 Wenchuan earthquake in the Beichuan area, Sichuan Province, China using satellite imagery and Google Earth. *Landslides* **6**, 153–159 (2009). doi: 10.1007/s10346-009-0147-6
10. British Geological Survey, Nepal earthquake response 2015 (2015); available at www.bgs.ac.uk/research/earthHazards/epom/NepalEarthquakeResponse.html.
11. R. N. Parker *et al*., Mass wasting triggered by the 2008 Wenchuan earthquake is greater than orogenic growth. *Nat. Geosci.* **4**, 449–452 (2011). doi: 10.1038/ngeo1154
12. C. Xu, X. Xu, X. Yao, F. Dai, Three (nearly) complete inventories of landslides triggered by the May 12, 2008 Wenchuan M_w 7.9 earthquake of China and their spatial distribution statistical analysis. *Landslides* **11**, 441–461 (2014). doi: 10.1007/s10346-013-0404-6
13. R. M. Yuan *et al*., Density distribution of landslides triggered by the 2008 Wenchuan earthquake and their relationships to peak ground acceleration. *Bull. Seismol. Soc. Am.* **103**, 2344–2355 (2013). doi: 10.1785/0120110233
14. E. L. Harp *et al*., Landslides and liquefaction triggered by the M 7.9 Denali Fault earthquake of 3 November 2002. *GSA Today* **13**, 4–10 (2003). doi: 10.1130/1052-5173(2003)013<0004:LALTBT>2.0.CO;2
15. R. W. Jibson, E. L. Harp, W. Schulz, D. K. Keefer, Landslides triggered by the 2002 Denali fault, Alaska, earthquake and the inferred nature of the strong shaking. *Earthq. Spectra* **20**, 669–691 (2004). doi: 10.1193/1.1778173
16. D. H. Shugar, J. J. Clague, The sedimentology and geomorphology of rock avalanche deposits on glaciers. *Sedimentology* **58**, 1762–1783 (2011). doi: 10.1111/j.1365-3091.2011.01238.x
17. F. C. Dai *et al*., Spatial distribution of landslides triggered by the 2008 M_s 8.0 Wenchuan earthquake, China. *J. Asian Earth Sci.* **40**, 883–895 (2011). doi: 10.1016/j.jseaes.2010.04.010
18. D. H. Shugar, B. T. Rabus, J. J. Clague, D. M. Capps, The response of Black Rapids Glacier, Alaska, to the Denali earthquake rock avalanches. *J. Geophys. Res.* **117** (F1), F01006 (2012). doi: 10.1029/2011JF002011
19. R. N. Parker *et al*., Spatial distributions of earthquake-induced landslides and hillslope preconditioning in the northwest South Island, New Zealand. *Earth Surf. Dynamics* **3**, 501–525 (2015). doi: 10.5194/esurf-3-501-2015
20. S. G. Evans *et al*., Catastrophic detachment and high-velocity long-runout flow of Kolka Glacier, Caucasus Mountains, Russia in 2002. *Geomorphology* **105**, 314–321 (2009). doi: 10.1016/j.geomorph.2008.10.008
21. W. Haeberli *et al*., The Kolka-Karmadon rock/ice slide of 20 September 2002: An extraordinary event of historical dimensions in North Ossetia, Russian Caucasus. *J. Glaciol.* **50**, 533–546 (2004). doi: 10.3189/172756504781829710
22. J. S. Kargel *et al*., Satellite monitoring of Pakistan's rockslide-dammed Lake Gojal. *Eos Trans. AGU* **91**, 394–395 (2010). doi: 10.1029/2010EO430002
23. V. Vilímek, M. L. Zapata, J. Klimes, Z. Patzelt, N. Santillán, Influence of glacial retreat on natural hazards of the Palcacocha Lake area, Peru. *Landslides* **2**, 107–115 (2005). doi: 10.1007/s10346-005-0052-6
24. M. Carey, Living and dying with glaciers: People's historical vulnerability to avalanches and outburst floods in Peru. *Glob. Planet. Change* **47**, 122–134 (2005). doi: 10.1016/j.gloplacha.2004.10.007
25. S. A. Dunning, N. J. Rosser, D. N. Petley, C. R. Massey, Formation and failure of the Tsatichhu landslide dam, Bhutan. *Landslides* **3**, 107–113 (2006). doi: 10.1007/s10346-005-0032-x
26. J. T. Weidinger, in *Natural and Artificial Rockslide Dams*, S. G. Evans, R. L. Hermanns, A. Strom, G. Scarascia-Mugnozza, Eds. (Springer, Berlin Heidelberg, 2011), pp. 243–277.
27. M. Geertsema, J. J. Clague, Pipeline routing in landslide-prone terrain. *Innovations* **15**, 17–21 (2011).
28. K. Hewitt, Disturbance regime landscapes: Mountain drainage systems interrupted by large rockslides. *Prog. Phys. Geogr.* **30**, 365–393 (2006). doi: 10.1191/0309133306pp486ra
29. Materials and methods are available as supplementary materials on *Science* Online.
30. Y. Ogata, Statistical models for earthquake occurrences and residual analysis for point processes. *J. Am. Stat. Assoc.* **83**, 9–27 (1988). doi: 10.1080/01621459.1988.10478560
31. D. K. Keefer, Investigating landslides caused by earthquakes—A historical review. *Surv. Geophys.* **23**, 473–510 (2002). doi: 10.1023/A:1021274710840
32. C. Xu, X. Xu, J. B. H. Shyu, Database and spatial distribution of landslides triggered by the Lushan, China Mw 6.6 earthquake of 20 April 2013. *Geomorphology* **248**, 77–92 (2015). doi: 10.1016/j.geomorph.2015.07.002
33. A. Jarvis, H. I. Reuter, A. Nelson, E. Guevara, Hole-filled seamless SRTM data v4 [International Centre for Tropical Agriculture (CIAT), 2008]; available at http://srtm.csi.cgiar.org.
34. P. Meunier, N. Hovius, J. A. Haines, Topographic site effects and the location of earthquake induced landslides. *Earth Planet. Sci. Lett.* **275**, 221–232 (2008). doi: 10.1016/j.epsl.2008.07.020
35. H. T. Chou, C. F. Lee, S. C. Chen, in *Earthquake-Induced Landslides: Proceedings of the International Symposium on Earthquake-Induced Landslides*, K. Ugai, H. Yagi, A. Wakai, Eds. (2013), pp. 45–57.
36. L. Chen *et al*., Liquefaction macrophenomena in the great Wenchuan earthquake. *Earthq. Eng. Eng. Vib.* **8**, 219–229 (2009). doi: 10.1007/s11803-009-9033-4
37. P. L. Moore, N. R. Iverson, D. Cohen, Ice flow across a warm-based/cold-based transition at a glacier margin. *Ann. Glaciol.* **50**, 1–8 (2009). doi: 10.3189/172756409789624319
38. H. Blatter, G. K. C. Clarke, J. Colinge, Stress and velocity fields in glaciers: Part II. Sliding and basal stress distribution. *J. Glaciol.* **44**, 457–466 (1998).
39. N. Bo, J. Persson, in *Sliding on Ice and Snow: Physical Principles and Applications* (Springer, Berlin, 1998), p. 391.
40. J. T. Weidinger, Predesign, failure and displacement mechanisms of large rockslides in the Annapurna Himalayas, Nepal. *Eng. Geol.* **83**, 201–216 (2006). doi: 10.1016/j.enggeo.2005.06.032
41. P. Deline *et al*., in *Snow and Ice-Related Hazards, Risks and Disasters*, W. Haeberli, C. Whiteman, J. F. Shroder, Eds. (Elsevier, Amsterdam, 2015), pp. 521–561.
42. M. Geertsema, M. Chiarle, in *Treatise on Geomorphology*, J. F. Shroder, M. Stoffel, R. A. Marston, Eds. (Elsevier, Amsterdam, 2013), vol. 7, pp. 217–222.
43. C. Liang, "Interferogram for ALOS2-track 48-swath ScanSARNominal14MHz; Feb 22, 2015 to May 3, 2015," UNAVCO InSAR Product, (2015).doi: 10.7283/S2KW2R
44. R. W. Jibson, E. L. Harp, "Field reconnaissance report of landslides triggered by the January 12, 2010, Haiti earthquake" (U.S. Geological Survey Open-File Report 2011-1023, Reston, VA, 2011).
45. E. L. Harp, R. W. Jibson, Landslides triggered by the 1994 Northridge, California earthquake. *Bull. Seismol. Soc. Am.* **86**, S319–S332 (1996).
46. J. Stöcklin, Geology of Nepal and its regional frame: Thirty-third William Smith Lecture. *J. Geol. Soc. London* **137**, 1–34 (1980). doi: 10.1144/gsjgs.137.1.0001
47. B. D. Collins, R. W. Jibson, "Assessment of existing and potential landslide hazards resulting from the April 25, 2015 Gorkha, Nepal earthquake sequence" (U.S. Geological Survey Open-File Report 2015-1142, Reston, VA, 2015).
48. J. P. McCalpin, E. W. Hart, "Ridge-top spreading features and relationship to earthquakes, San Gabriel Mountains region, Southern California - Part B: Paleoseismic investigations of ridge-top depressions," *Final Technical Report, Contract 1434-HQ-GR-1026, National Earthquake Hazards Reduction Program* (U.S. Geological Survey, 2002).
49. R. D. Nason, in *The San Fernando, California, earthquake of February 9, 1971, U.S. Geological Survey Professional Paper 733* (U.S. Geological Survey, Washington, DC, 1971), pp. 97–98.
50. S.-J. Lee, D. Komatitsch, B.-S. Huang, J. Tromp, Effects of topography on seismic-wave propagation: An example from northern Taiwan. *Bull. Seismol. Soc. Am.* **99**, 314–325 (2009). doi: 10.1785/0120080020
51. W. W. Immerzeel, L. Petersen, S. Ragettli, F. Pellicciotti, The importance of observed gradients of air temperature and precipitation for modeling runoff from a glacierized watershed in the Nepalese Himalayas. *Water Resour. Res.* **50**, 2212–2226 (2014). doi: 10.1002/2013WR014506
52. K. Fujita, T. Nuimura, Spatially heterogeneous wastage of Himalayan glaciers. *Proc. Natl. Acad. Sci. U.S.A.* **108**, 14011–14014 (2011). doi: 10.1073/pnas.1106242108; pmid: 21808042
53. S. Ragettli *et al*., Unraveling the hydrology of a Himalayan catchment through integration of high resolution in situ data and remote sensing with an advanced simulation model. *Adv. Water Resour.* **78**, 94–111 (2015). doi: 10.1016/j.advwatres.2015.01.013
54. C. Cadwalladr, "Nepal earthquake: The village wiped off the map in a few terrifying seconds," *The Guardian*, 16 May 2015.
55. ICIMOD, *Glacial Lakes and Glacial Lake Outburst Floods in Nepal* (International Centre for Integrated Mountain Development, Kathmandu, Nepal, 2011), pp. 99.
56. J. J. Clague, S. G. Evans, A review of catastrophic drainage of moraine-dammed lakes in British Columbia. *Quat. Sci. Rev.* **19**, 1763–1783 (2000). doi: 10.1016/S0277-3791(00)00090-1
57. K. Fujita *et al*., Potential flood volume of Himalayan glacial lakes. *Nat. Hazards Earth Syst. Sci.* **13**, 1827–1839 (2013). doi: 10.5194/nhess-13-1827-2013
58. S. Ma, R. J. Archuleta, M. T. Page, Effects of large-scale topography on ground motions as demonstrated by a study of the San Gabriel Mountains, Los Angeles, California. *Bull. Seismol. Soc. Am.* **97**, 2066–2079 (2007). doi: 10.1785/0120070040
59. A. C. Byers, D. C. McKinney, E. A. Byers, "Post-earthquake assessment: Imja, Tsho Rolpa, and Thulagi glacial lakes in Nepal" (U.S. Agency for International Development, 2015).
60. W. Schwanghart *et al*., Repeated catastrophic valley infill following medieval earthquakes in the Nepal Himalaya. *Science* **351**, 147–150 (2015).
61. A. Arendt *et al*., "Randolph Glacier Inventory—A dataset of global glacier outlines: version 4.0" (Global Land Ice Measurements from Space, Boulder, CO, 2014).
62. U.S. Geological Survey, Earthquake Hazards Program (2015); available at http://earthquake.usgs.gov.
63. M. R. Dhital, *Geology of the Nepal Himalaya—Regional Geology Reviews* (Springer, 2015).
64. L. S. Walsh, A. J. Martin, T. P. Ojha, T. Fedenczuk, Correlations of fluvial knickzones with landslide dams, lithologic contacts, and faults in the southwestern Annapurna Range, central Nepalese Himalaya. *J. Geophys. Res.* **117**, F01012 (2012). doi: 10.1029/2011JF001984

ACKNOWLEDGMENTS

J.S.K., G.J.L., and U.K.H. thank the NASA SERVIR Applied Science Team and NASA Cryosphere Program for support. D.H.S. thanks the Hakai Institute for support. Part of this research was sponsored by the NASA Earth Surface and Interior focus area and performed at the Jet Propulsion Laboratory, California Institute of Technology. We gratefully acknowledge support from several "citizen scientists" who provided key observations and reports from various locations in Nepal: D. Rai, J. B. Rai, N. Sapkota, M. Dhan Rai, and M. Gotame, who made on-site inspections and photo documentation of Thulagi (Dona) Lake, Rolpa Lake, Kali Gandaki, and "Lower Pisang" landslide dammed lake. ASTER data are courtesy of NASA/GSFC/METI/Japan Space Systems, the U.S./Japan ASTER Science Team, and GLIMS. We especially laud DigitalGlobe's decision to acquire and make available a vast volume of data for analysis related to Gorkha earthquake response. We thank C. Liang for processing the ALOS-2 wide-swath interferogram. Original ALOS-2 data are copyright 2015 JAXA. This study was partially supported by core funds of ICIMOD contributed by the governments of Afghanistan, Australia, Austria, Bangladesh, Bhutan, China, India, Myanmar, Nepal, Norway, Pakistan, Switzerland, and the United Kingdom. This study was partially supported by the Hundred Talents Program of the Chinese Academy of Sciences (grant 784) and the National Natural Science Foundation of China (grants 41431070 and 41321063). The two chief databases produced by this work are available at ICIMOD (landslides, http://rds.icimod.org/Home/DataDetail?metadataId=24055; and glacial lakes, http://rds.icimod.org/Home/DataDetail?metadataId=24065).

SUPPLEMENTARY MATERIALS

www.sciencemag.org/content/351/6269/aac8353/suppl/DC1
Materials and Methods
Figs. S1 to S6
Tables S1 to S3

20 June 2015; accepted 27 November 2015
Published online 17 December 2015
10.1126/science.aac8353